A Simple Self-assembling System of Melittin for Hepatoma Treatment

Xin Jin
China Pharmaceutical University
Qing Yang
Suqian First Hospital
Jie Song
Nanjing University of Chinese Medicine
Zhenhai Zhang (david23932@163.com)
Jiangsu Province Academy of Traditional Chinese Medicine

Research Article

Keywords: self-assembly, peptide, hepatoma therapy, formation mechanism

Posted Date: March 17th, 2022

DOI: https://doi.org/10.21203/rs.3.rs-1447025/v1

Abstract

Hepatoma is a serious public health concern. New attempts are urgently needed to solve this problem. Melittin, a host defense peptide derived from the venom of honeybees, has noteworthy hemolysis and non-specific cytotoxicity in clinical applications. Here, the self-assembly of melittin and vitamin E-succinic acid-$(glutamate)_{12}$ (VG) was fabricated via noncovalent π-stacking and hydrogen bonding interactions by an environment-friendly method without the use of “toxic” solvents. As expected, the designed self-assembly (denoted as M/VG nanoparticles) exhibits a uniform morphology with a particle size of approximately 60 nm and a zeta potential of approximately −26.8 mV. Furthermore, added VG significantly decreased hemolytic activity, increased tumor-targeted effects, promoted the cellular uptake, and accelerate apoptosis. Our research provides a promising strategy for the development of natural self-assembled biological peptides for clinical application, particularly for transforming toxic peptides into safe therapeutic systems.

Introduction

Almost 906,000 new liver cancer cases are reported, and approximately 830,000 patients die from liver cancer annually, as presented in the global cancer statistics 2020. It is the third most common cancer in and is associated with high mortality [1]. Therefore, it is important to make new attempts to solve this problem. Melittin (GIGAVLKVLTTGLPALISWIKRKRQQ-NH2, M) is the main active pharmacological peptide component of bee venom; it consists of 40–50% of the dry weight of bee venom [2]. The relative results of a clinical trial of 40 patients with hepatocellular carcinoma treated with melittin for clinical application indicated that the disease control rate was approximately 70% [3]. However, melittin exhibits not only anti-tumor functions, but also non-specific cytotoxicity and non-negligible hemolytic performance.

Two strategies are often used to address these problems. The first is chemical modification to increase specificity and decrease hemolysis [4]. The other is physicochemical encapsulation by various nanocarriers, such as classical liposomes [3], polyelectrolyte nanocarriers [5], polymeric nanocarriers [6], redox-sensitive nanocomplexes [7], pH-sensitive micelles [8], microneedles [9], inorganic materials [10], and hydrogels [11]. Modification or complex multifunctional carriers are often limited by the complexity of the production process, high cost, and repeatability, which hinder their clinical applications. Before melittin can be used in the clinic, further investigations are required to maintain a balance between therapeutic benefits, toxicity risks, and preparation technologies [12].

Self-assembly is a common process in biology, which is the basis for various complex biological structures, such as DNA, microtubules, and vesicles [13]. Compared to covalent polymers, peptide-based self-assembly has advantages such as easy preparation, biodegradability, and biocompatibility [14]. Moreover, peptide molecules in the blood are usually removed by enzyme degradation, glomerular filtration, and uptake by the reticuloendothelial system [15]. Nevertheless, the self-assembled nanoparticles, endow peptides with high stability, good biological distribution, and tumor-targeted effects to address unmet clinical needs [16, 17].

Bian et al. recently reported that electrostatic co-assembly behavior exists in oppositely charged small molecules and nanoparticles [18]. In the present study, we observed the same phenomenon and designed a peptide-assembled nanosystem based on melittin and vitamin E-succinic acid-(glutamate)$_{12}$ (VG) for the treatment of liver cancer. The novel and environment-friendly approach was formed without the use of organic solvents. Vitamin E-succinic acid-(glutamate)$_{12}$ (VG) interacts with each other to form a hydrophobic core, which interact with melittin on the surface attached to the core of the nanoparticle through noncovalent π-stacking and hydrogen bonding. The fabricated self-assembled system decreased the hemolysis and increased the dosage of administration in vivo. Furthermore, the nano system could also promote the cellular uptake, accumulation in tumor tissues, and apoptosis of HepG2 cells in vivo. Compared with free melittin, M/VG nanoparticles could administrate with high does, remarkably accumulate in tumor tissues, exhibit the superior anti-tumor effects against HepG2 cells with better biocompatibility. Compared to previously reported self-assembly systems of melittin [19–21], this plain system consists of peptides sourced from amino acids, the basic structures of the human body. This quality makes it suitable for use in clinical applications, particularly for creating anti-tumor peptides.

Materials And Methods

Materials

Melittin was synthesized by Nanjing Peptide Industry Biotechnology Co., Ltd. (Nanjing, China). Vitamin E-succinic acid-(glutamate)$_{12}$ was synthesized by China Peptide Industry Biotechnology Co., Ltd. (Shanghai, China). NH_2-Cy5 was purchased from Meilun Biotechnology Co., Ltd. (Dalian, China). HepG2 cells, RPMI-1640 medium, fetal bovine serum, MTT, apoptosis detection kit, and Ki67 detection kit were obtained from KeyGen Biotech Co., Ltd. (Nanjing, China).

Molecular dynamics (MD) simulations

The self-assembly process of the M/VG nanoparticles was analyzed using molecular dynamics simulations. The PDB ID of melittin is 2mlt. The parameters for the VG molecules were constructed using Amber Tools. An artificial box containing 10 melittin and 10 VG molecules was designed in a TIP3P water box with a side length of 1 nm. This system was optimized for 5000 steps with 100 ps in the NVT and NPT systems. Then, the temperature was kept constant at 298 K with a relaxation time of 10 ps at 1 bar for a total simulation time of 15 ns. The cutoff distance was 1.2 nm. The simulation time step was 2 fs. Molecular dynamics simulations were performed using the Gaussian09 program based on Gromacs2018.

Preparation and characterization of M/VG nanoparticles

Initially, melittin was added to deionized water to form a solution, then mixed with different ratios of vitamin E-succinic acid-(glutamate)$_{12}$ (dissolved in buffer solution). The blend was efficiently stirred with a magnetic stirrer and further dispersed by bath sonication. Cy5-labeled nanoparticles were prepared by the above-mentioned technique using Cy5-labeled melittin and vitamin E-succinic acid-(glutamate)$_{12}$. To

prepare fluorescently labeled melittin, melittin was conjugated with NH2-Cy5 in accordance with a previous report [19].

The negative zeta potentials of different M/VG nanoparticles were measured and optimized using a Zetasizer (Nano ZS, Malvern Instruments, UK). The hydrodynamic size of the optimized M/VG nanoparticles was examined using dynamic light scattering (BT-90, Bettersize Instruments Ltd., China). Transmission electron microscopy (TEM) was used to observe the morphology of the optimized M/VG nanoparticles (JEM-2100, JEOL Ltd., Japan).

Circular dichroism (CD) spectrum analysis

The CD spectra of free melittin and M/VG nanoparticles were analyzed at the same concentration of melittin (0.5 mg/mL) in a quartz cell at 200 to 280 nm with a path length of 0.1 cm.

Hemolysis evaluation

The whole blood of rats was obtained and centrifuged to collect red blood cells (RBCs). Then, melittin or M/VG nanoparticles at various concentrations were added to the RBC suspension and incubated for analysis using a microplate reader.

MTT assay

The MTT assay was used to evaluate the anti-tumor effect on HepG2 cells *in vitro*. Briefly, HepG2 cells were seeded in 96-well plates, cultured for 24 h, and incubated with melittin or M/VG nanoparticles for another 48 h. Then, MTT solution was added, and the cells were cultured for another 4 h. Finally, after removal of the medium, DMSO was added to each well and the absorbance was measured at 570 nm using a microplate reader.

Wound healing experiment

HepG2 cells were seeded in 24-well plates and cultured for 12 h. Afterward, the HepG2 cells were scratched using A 20 μl micropipette tip to form wounds. This was recorded as 0 h. Then, the cells were treated with different group for 48 h. Wound images were recorded and evaluated at both 0 and 48 h.

Apoptosis assay

HepG2 cells were cultured for 24 h and incubated with free medium, melittin, or M/VG nanoparticles. After 48 h, the cells were digested with trypsin, washed with phosphate-buffered saline, stained using an apoptosis detection kit, and analyzed using flow cytometry.

In vitro uptake analysis

To investigate the difference in cellular uptake between melittin and M/VG nanoparticles, HepG2 cells were cultured, incubated with Cy5-labeled melittin or Cy5-labeled nanoparticles, and images were

captured at 1 h and 4 h using a confocal laser microscope. During treatment with Cy5-labeled melittin or Cy5-labeled nanoparticles for 4 h, flow cytometry was used for quantitative analysis.

In vivo imaging

When tumor volumes grew to approximately 150 mm^3, Cy5-labeled melittin or Cy5-labeled nanoparticles were intravenously injected into male BALB/c mice via the tail vein. After injection, the fluorescent signal of Cy5 was recorded at 1, 2, 4, 8, and 24 h. Tumor tissues and major organs were obtained and observed at the end of the experiments using an optical imaging platform.

In vivo anti-tumor effect and safety evaluation

To further explore the therapeutic effect *in vivo*, mice were divided into five groups, when tumor volumes reached 50 mm^3. Four groups were injected with saline (blank control), melittin (2.5 mg/kg), M/VG nanoparticles (2.5 mg/kg), or M/VG nanoparticles (5 mg/kg) via the tail vein every three days for a total of four doses. The positive control was orally administered sorafenib (30 mg/kg) daily for a total of 12 doses. Tumor size was calculated every three days.

After treatment, tumor tissues and the major organs were collected for further hematoxylin and eosin (H&E) or Ki67 analysis. Fresh blood was further analyzed, and biochemical parameters were measured.

Statistical analysis

All data are shown as mean ± standard deviation and further analyzed using the Student's *t*-test. Differences were considered significant at $P < 0.05$.

Results And Discussion

Self-Assembly Mechanism

The structures of melittin and VG are shown in Fig. 1A. Molecular dynamics (MD) simulation snapshots depicting the time evolution between melittin and VG Initially, melittin and VG began to aggregate within 3 ns. Subsequently, the self-assembled nanoparticles became stable after 6 ns, as shown in Fig. 1B.

In the designed self-assembly system, the interaction was mainly composed of hydrogen bonds (Fig. 1C) and stacking effects (Fig. 1D). The van der Waals force in M/VG nanoparticles declined significantly with MD beginning, gradually stabilized after 6 ns, and stabilized in the range of − 2000 kJ/mol, indicating that the stacking effect (dominant by van der Waals force) in the designed self-assembly is gradually strengthened (Fig. 2A). Figure 2B shows the changes in the number of hydrogen bonds during the self-assembly process. In the first 6 ns, the intermolecular hydrogen bonds in the designed system were approximately 10. When simulated from 6 to 12 ns, the number of hydrogen bonds increased and

stabilized at approximately 10–15. After 12 ns, the number of hydrogen bonds further increased and stabilized at 15–20. The electrostatic force energy (Fig. 2C) showed the same trend as the number of hydrogen bonds, since as the number of hydrogen bonds increased, the electrostatic force energy was gradually stable.

In the first 3 ns, the radius of gyration decreased significantly from about 2.8 nm to about 2.6 nm. After approximately 3 ns, the radius of gyration of the t-system gradually stabilized. The results show that the system was assembled successfully after 3 ns (Fig. 2D).

Figure 2E indicates that in the first 3 ns, the root-mean-square deviation (RMSD) of the clustering system was the largest at approximately 1.0 nm. From 3 ns to 8 ns, the RMSD between cluster systems decreased to approximately 0.7 nm. After 8 ns, the RMS deviation between clustering systems gradually tended to 0.4 nm. The above results confirmed that with the advancement of simulation time, the RMS deviation in clusters gradually decreased, resulting in self-assembly behavior and finally forming a stable nanoparticle structure. The relative results are consistent with the cluster behavior shown in Fig. 2F.

After forming a stable structure, the interactions between melittin and VG (Fig. 3A) were mainly based on hydrogen bonds and stacking interactions. GLY3, ALA4, and VAL5 in melittin interacted with the carbonyl or carboxyl of glutamate in VG via hydrogen bonding through NH-O interactions. LEU9 in melittin interacted with the benzene ring of vitamin E in VG by stacking interactions through CH-π interactions. ILE2 and VAL5 in melittin interacted with the benzene ring of vitamin E in VG by stacking interactions through CH-CH interactions. The interactions between VG and VG (Fig. 3B) were also mainly based on hydrogen bonds (OH-O and OH-N between glutamates) and stacking interactions (CH3-π and CH3-CH3 between vitamin E). The interactions between melittin and melittin (Fig. 3C) were also mainly based on hydrogen bonds (THR10 with PRO14 or SER18 by OH-O, LEU6 with SER18 by O-HO), and stacking interactions (LEU9-ILE17, PRO14-PRO14, and SER18-LEU6).

Characterization of M/VG nanoparticles

We optimized the mole ratio of melittin to VG in the self-assembly by zeta potentials, as shown in Fig. 4A. This was conducted because shielding the positive charges of melittin is key to decrease its hemolysis. With an increase in VG, the electric charge of melittin was reversed. To optimize the self-assembled nanoparticles of melittin and VG (mole ratio, 1:1), the potential of melittin (+ 19.6 mV) was transformed into − 26.8 mV, which was selected due to stable negative potential (Fig. 4B). The surface charge of M/VG nanoparticles was negative, which helped the self-assemble to escape from the recognition of the reticuloendothelial system and increased the retention time *in vivo* [22]. The hydrodynamic size of the M/VG nanoparticles was 63.4 nm as shown in Fig. 4C. As shown in Fig. 4D, the M/VG nanoparticles are spherical particles of approximately 30 nm. TEM revealed that the nanoparticles had smaller hydrodynamic size, which may be because TEM assesses solid particle sizes without a water layer, which is different from the hydrodynamic size. The average sizes of M/VG nanoparticles were smaller than the inter-endothelial gaps in most tumor vessels (380–780 nm), which is small enough to passively permeate into the tumor [23, 24].

CD spectrum characteristics

The CD spectra in Fig. 4E reveal that melittin has an α-helical configuration with negative peaks at approximately 209 and 220 nm. The results also demonstrated that VG converts the conformation of melittin because of the random coil of the M/VG nanoparticles. Previous reports have implied that melittin has an α-helical structure that easily binds to lipid membranes [25, 26]. Therefore, the change in the α-helical signal into a random coil suggests that M/VG nanoparticles might have low hemolysis.

Hemocompatibility of M/VG nanoparticles

As mentioned above, VG promoted the electric charge conversion of melittin by self-assembly (Fig. 4B). Shielding the positive charge of melittin is crucial for decreasing the interaction with RBCs. [11] Furthermore, after self-assembly into M/VG nanoparticles, the α-helical melittin changed into a random coil, probably yielding a decreased hemolytic effect of melittin (Fig. 4E). *In vitro* hemolytic evaluation indicated that melittin at a concentration of 20 μg/mL could lyse almost 50% RBCs, whereas at equal concentrations of melittin in M/VG nanoparticles, it only exhibited 12% hemolysis (Fig. 4F), further confirming that the fabricated self-assembly could remarkably increase the hemocompatibility of melittin.

MTT assay

The MTT assay was performed to evaluate the anti-tumor effect on HepG2 cells *in vitro*. The relative results indicated that the viability of melittin and M/VG nanoparticles-treated cells decreased significantly as the concentration of melittin increased (Fig. 5A). Meanwhile, the half-maximal inhibitory concentration (IC_{50}) of M/VG nanoparticles was calculated as 2.13 μg/mL, a decrease of 55.16%, compared with that of melittin (4.75 μg/mL). This observation might be attributed to the different cellular uptake mechanisms of melittin and M/VG nanoparticles in HepG2 cells. Designed M/VG nanoparticles not only have good hemocompatibility but also have an effective therapeutic impact.

Wound healing assay

The effect of M/VG nanoparticles on HepG2 cell motility was evaluated using a scratch wound healing assay. As shown in Fig. 5B, HepG2 cells in the control group showed a significant motor aggregation phenotype. Both melittin and M/VG nanoparticles significantly inhibited cell motility. Compared with the melittin group, M/VG nanoparticles presented a lower healing rate, which decreased by 28.41%.

Apoptosis assay

HepG2 cells in the control group exhibited low apoptosis levels, as shown in Fig. 6A. Conversely, the M/VG nanoparticles significantly induced apoptosis in HepG2 cells and increased by 14.6%, compared with the melittin group (Fig. 6A).

Cellular uptake *in vitro*

As shown in Fig. 6B, within the first 1h, the cellular uptake of Cy5-labeled melittin and Cy5-labeled nanoparticles was low (Fig. 6B). As time increased, compared to Cy5-labeled melittin, HepG2 cells treated with Cy5-labeled nanoparticles displayed higher fluorescence signals at 4 h, indicating increased capture of Cy5-labeled nanoparticles (Fig. 6C). Furthermore, for quantitative analysis, the cellular uptake results in HepG2 cells demonstrated that Cy5-labeled nanoparticles could promote the uptake, which was 1.06 times higher than that of Cy5-labeled melittin (Fig. 6D).

In vivo imaging

To assess the tumor-targeting capability of Cy5-labeled nanoparticles, the biodistribution of Cy5-labeled melittin and Cy5-labeled nanoparticles, were both monitored. As shown in Fig. 7, Cy5-labeled melittin had insufficient tumor-targeting capacity and non-specific distribution. Conversely, Cy5-labeled nanoparticles first presented a fluorescence signal at 2 h in the tumor location after injection. As time elapsed, stronger fluorescent signals in the tumor region reached a plateau at 4 h. Notably, the Cy5-labeled nanoparticles were stably retained in the tumors and could still be detected after 24 h, validating a significant systemic long circulation and tumor-targeting capacity. Meanwhile, the *ex vivo* fluorescence imaging of tumor tissues and main organs as shown in Fig. 7 also indicated that Cy5-labeled nanoparticles could increase the accumulation of melittin in tumors, which is consistent with the *in vivo* imaging results. Furthermore, only lower deposition was detected in the liver, lung, and kidney. More importantly, Cy5-labeled nanoparticles showed a longer liver retention time, which may be a potential application for hepatocellular carcinoma. Notably, rapid clearance was found for the Cy5-labeled melittin, and fluorescence signals of the Cy5-labeled melittin group were less than those of the Cy5-labeled nanoparticles group, especially in the tissues after 24 h.

In vivo anti-tumor evaluation

Encouraged by the decreased hemolysis *in vitro* and increased tumor accumulation *in vivo*, an *in vivo* anti-tumor evaluation was performed. The limited tumor growth inhibition (39.86%) of melittin was observed, which could be attributed to the rapid clearance of the injections in the circulation system and lower affinity with the HepG2 cells. Compared to the melittin group, the self-assembled nanoparticles showed a longer retention time and specific tumor permeation (Fig. 7). As expected, the tumor growth curve and tumor images showed that M/VG nanoparticles dramatically suppressed tumor growth (Fig. 8A and 8B). At the end of the experiments, compared with the control group, mice treated with M/VG nanoparticles showed a 70.19% decrease in tumor volume for M/VG nanoparticles (2.5 mg/kg) and 92.96% inhibition for M/VG nanoparticles (5 mg/kg). In addition, even compared to the sorafenib group (positive control), the M/VG nanoparticles (5 mg/kg) group also showed a dramatic decrease in tumor size by 60.42%. When treated with melittin (2.5 mg/kg), hemolysis began from the bottom of the caudal vein, and melittin was gradually injected from the bottom to the top of the mouse tail. Therefore, the tails of the melittin (2.5 mg/kg) group showed severe tissue necrosis. Interestingly, the M/VG nanoparticle group exhibited no significant tail injury, even at a high dose of 5 mg/kg (Fig. 8C).

H&E and Ki67 staining of tumor tissues were chosen for histological evaluation (Fig. 8D). In the control group, tumor cells were large, polygonal, or almost round with obvious nucleoli and were easily observed. Fibrous tissues divided the tumor cells into small nests. For melittin and M/VG nanoparticles (2.5 mg/kg) groups, tumor cells were distributed diffusely without significant nest structure. Furthermore, when treated with M/VG nanoparticles (5 mg/kg) or sorafenib, tumor cells died significantly with no nuclear and dull cytoplasm eosin staining. Ki67 is a marker of tumor cell proliferation The proportion of Ki67 positive cells in the control group was significantly higher than that in the M/VG nanoparticles (5 mg/kg) group. The results showed that treatment with M/VG nanoparticles (5 mg/kg) induced malignant hepatoma proliferation (Fig. 8D).

Additionally, for histological evaluation, compared with the control, there were no significant histological changes in the major tissues in other treatment groups (Fig. 9). Meanwhile, melittin caused a significant decrease in hematocrit, demonstrating that melittin interacts with hemocytes *in vivo*; however, M/VG nanoparticles exhibited similar hemocyte levels as the control group. These results collectively indicate that M/VG nanoparticles can be used safely without causing evident hematotoxicity (Fig. 10).

Conclusions

Collectively, melittin self-assembled with VG to form nanoparticles using a simple environment-friendly preparation method. Melittin interacted with VG on the surface of spherical nanoparticles via hydrogen bond interactions and π–π stacking interactions. Both *in vitro* uptake assays and *in vivo* imaging revealed that melittin accumulation in HepG2 cells significantly increased after self-assembly. Importantly, after forming the M/VG nanoparticles, compared with free melittin, hemolysis decreased significantly and dosage of administration increased remarkably. Therefore, M/VG nanoparticles (5 mg/kg) exhibited superior anti-tumor effects against HepG2 cells by promoting apoptosis both *in vitro* and *in vivo*. Tumor volumes decreased by 92.96% compared with the control, indicating a potent therapeutic effect. In contrast to previously reported melittin systems, our research supports a simple and promising self-assembling system to apply more naturally bioactive peptides for targeted precision therapy, particularly to turn toxicants into safe therapeutic systems.

Abbreviations

VG Vitamin E-succinic acid-$(glutamate)_{12}$

M/VG nanoparticles Melittin and vitamin E-succinic acid-$(glutamate)_{12}$ self-assembly

TEM Transmission electron microscopy

CD Circular dichroism

RBC Red blood cells

H&E Hematoxylin and eosin

MD Molecular dynamics

RMSD Root-mean-square deviation

Declarations

Ethics approval and consent to participate

All animal experiments were approved by the Animal Ethics Committee of Jiangsu Province Academy of Traditional Chinese Medicine.

Consent for publication

All authors gave their consent for publication.

Availability of data and materials

All data related to the manuscript are available in the manuscript in the form graphs and figures.

Competing interests

There are no conflicts of interest to declare.

Funding

The authors acknowledge financial support from Medical Research Project of Jiangsu Provincial Health Commission (H2019096). This study was also supported by Suqian Sci & Tech Program (K201908), National Natural Science Foundation of China (Grant No. 81873055), and Six Talent Peak Projects in Jiangsu Province (SWXY-010-2019).

Authors' contributions

XJ and ZHZ conceived and designed the project. XJ and QY carried out the experiments’ preparation and characterization. XJ and JS carried out cell delivery experiments. JS performed animal experiments. XJ, JS and ZHZ wrote and edited the manuscript. All authors contributed to the manuscript revision. All authors read and approved the final manuscript.

Acknowledgements

Not applicable

References

1. Sung H, Ferlay J, Siegel RL, Laversanne M, Soerjomataram I, Jemal A, Bray F, Global cancer statistics 2020: GLOBOCAN estimates of incidence and mortality worldwide for 36 Cancers in 185 Countries, CA A Cancer Journal for Clinicians. 2021; 71(3):209-249.
2. Kim W, Bee venom and its sub-components: characterization, pharmacology, and therapeutics, Toxins.2021;13:191.
3. Mao J, Liu S, Ai M, Wang Z, Wang D, Li X, Hu K, Gao X, Yang Y, A novel melittin nano-liposome exerted excellent anti-hepatocellular carcinoma efficacy with better biological safety, J Hematol Oncol.2017; 10(1):71-74.
4. Lyu C, Fang F, Li B, Anti-tumor effects of melittin and its potential applications in clinic, Curr Protein Pept Sci. 2018; 19(3):240-250.
5. Motiei M, Aboutalebi F, Forouzanfar M, Dormiani K, Mirahmadi-Zare SZ, Smart co-delivery of mir-34a and cytotoxic peptides (ltx-315 and melittin) by chitosan based polyelectrolyte nanocarriers for specific cancer cell death induction, Mat Sci Eng C. 2021; 128:112258.
6. Lv S, Sylvestre M, Song K, Pun SH, Development of d-melittin polymeric nanoparticles for anti-cancer treatment, Biomaterials. 2021; 277(73):121076.
7. Cheng B, Xu P, Redox-sensitive nanocomplex for targeted delivery of melittin, Toxins. 2020; 12: 582-594.
8. Peeler DJ, Thai SN, Cheng Y, Horner PJ, Sellers DL, Pun SH, pH-sensitive polymer micelles provide selective and potentiated lytic capacity to venom peptides for effective intracellular delivery, Biomaterials. 2019;192:235-244.
9. Du G, He P, Zhao J, He C, Sun X, Polymeric microneedle-mediated transdermal delivery of melittin for rheumatoid arthritis treatment, J Control Release. 2021; 336:537-548.
10. Li YW, Xu N, Zhu WH, Wang L, Liu B, Zhang JX, Xie ZG, Liu WS, Nanoscale melittin@zeolitic imidazolate frameworks for enhanced anticancer activity and mechanism analysis, ACS Appl. Mater. Interfaces. 2018; 10(27): 22974–22984
11. Zhou YH, Ye T, Ye CZ, Wan C, Yuan SY, Liu YS, Li TY, Jiang FG, Lovell JF, Jin HL, Chen J, Secretions from hypochlorous acid-treated tumor cells delivered in a melittin hydrogel potentiate cancer immunotherapy, Bioact Mater. 2021; 9: 541-553.
12. Zhou J, Wan C, Cheng J, Huang H, Jin H, Delivery strategies for melittin-based cancer therapy, ACS Appl. Mater. Interfaces. 2021; 13(15):17158–17173.
13. Lai YT, King NP, Yeates TO, Principles for designing ordered protein assemblies, Trends Cell Biol, 2012;22: 653-61.
14. Wang Y, Zhang X, Wan K. et al. Supramolecular peptide nano-assemblies for cancer diagnosis and therapy: from molecular design to material synthesis and function-specific applications. Journal of Nanobiotechnology, 2021;19:253-284.
15. Green BD, Gault VA, Mooney MH, Irwin N, Harriott P, Greer B, Bailey CJ, O'Harte FP, Flatt PR, Degradation, receptor binding, insulin secreting and antihyperglycaemic actions of palmitate-derivatised native and Ala8-substituted GLP-1 analogues, Biol. Chem. 2004; 385(2): 169–177.

16. Chen L, Lian JF, Peptide fibrils with altered stability, activity, and cell selectivity, Biomacromolecules. 2013; 14(7): 2326–2331.
17. Tu Z, Hao J, Kharidia R, Meng XG, Liang JF, Improved stability and selectivity of lytic peptides through self-assembly, Biochem. Biophys. Res. Commun. 2007; 361(3): 712–717.
18. Bian T, Gardin A, Gemen J, Houben L, Perego C, Lee B, Elad N, Chu ZL, Pavan GM, Klajn R, Electrostatic co-assembly of nanoparticles with oppositely charged small molecules into static and dynamic superstructures, Nat. Chem. 2021;13:940–949.
19. Jia HR, Zhu YX, Liu X, Pan GY, Wu FG, Construction of dually responsive nanotransformers with nanosphere–nanofiber–nanosphere transition for overcoming the size paradox of anticancer nanodrugs, ACS Nano. 2019; 13(10):11781–11792.
20. Jia HR, Zhu YX, Xu KF, Wu FG, Turning toxicants into safe therapeutic drugs: cytolytic peptidephotosensitizer assemblies for optimized in vivo delivery of melittin, Advanced Healthcare Materials. (2018; 7(16):1800380.
21. Qiao HZ, Dong F, Lei Z, Gu X, Di L, Nanostructured peptidotoxins as natural pro-oxidants induced cancer cell death via amplification of oxidative stress, ACS Appl. Mater. Interfaces. 2018; 10(5): 4569–4581.
22. Cheng B, Thapa B, Remant KC, Xu PS, Dual secured nano-melittin for the safe and effective eradication of cancer cells, J Mater Chem B Mater Biol Med. 2014; 3(1):25-29.
23. Chen G, Roy I, Yang C, Prasad PN, Nanochemistry and Nanomedicine for Nanoparticle-based Diagnostics and Therapy, Chem. Rev. 2016; 116(5):2826–85.
24. Jain RK, Stylianopoulos T, Delivering nanomedicine to solid tumors, Nat. Rev. Clin. Oncol. 2010; 7 (11): 653–64.
25. Toraya S, Nishimura K, Naito A, Dynamic structure of vesicle-bound melittin in a variety of lipid chain lengths by solid-state NMR. Biophysical Journal. 2004; 87:3323–3335.
26. Lundquist A, Wessman P, Rennie AR, Edwards K, Melittin–lipid interaction: a comparative study using liposomes, micelles and bilayerdisks, Biochim. Biophys. Acta. 2008;1778:2210.

Figures

Figure 1

Structures of melittin and VG (A) and its MD simulation for 15 ns (B). In the designed self-assembly system, the interaction is mainly composed of hydrogen bonds (C) and stacking effects (D).

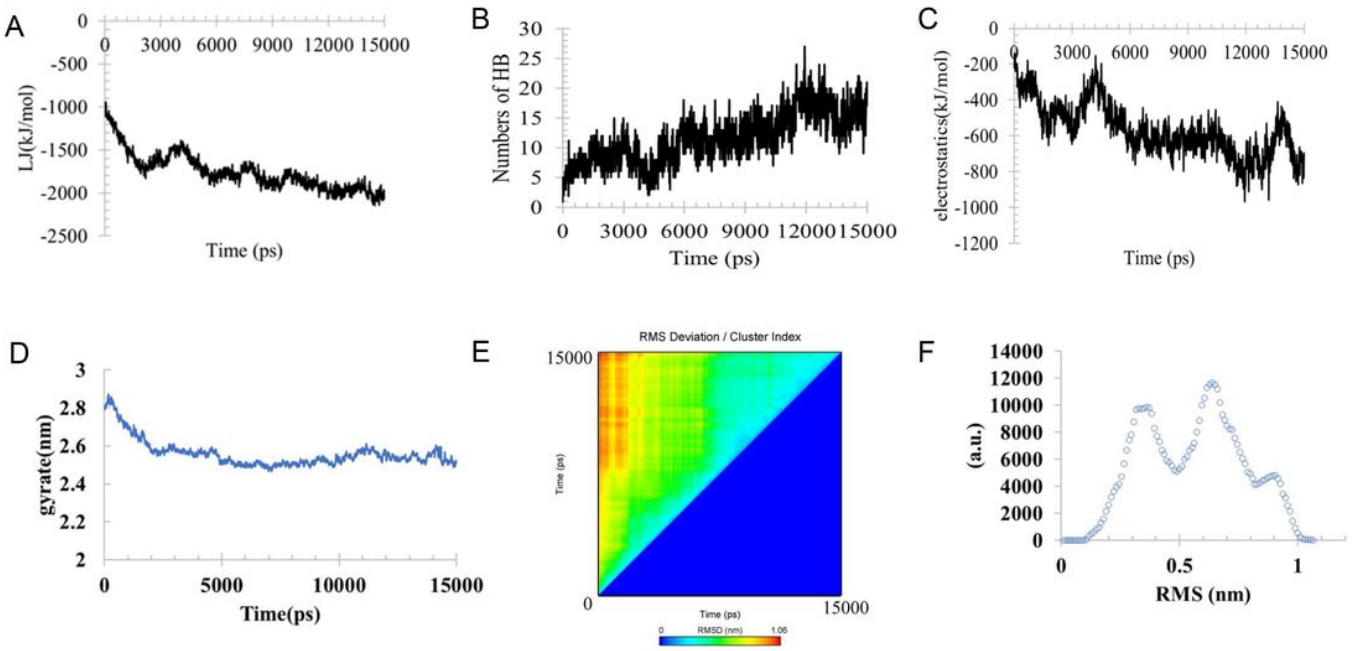

Figure 2

Change in van der Waals force (A), hydrogen bonds, (B) and electrostatic force energy (C), radius of gyration (D), root-mean-square deviation (E), and cluster behavior (F) in the self-assembly process.

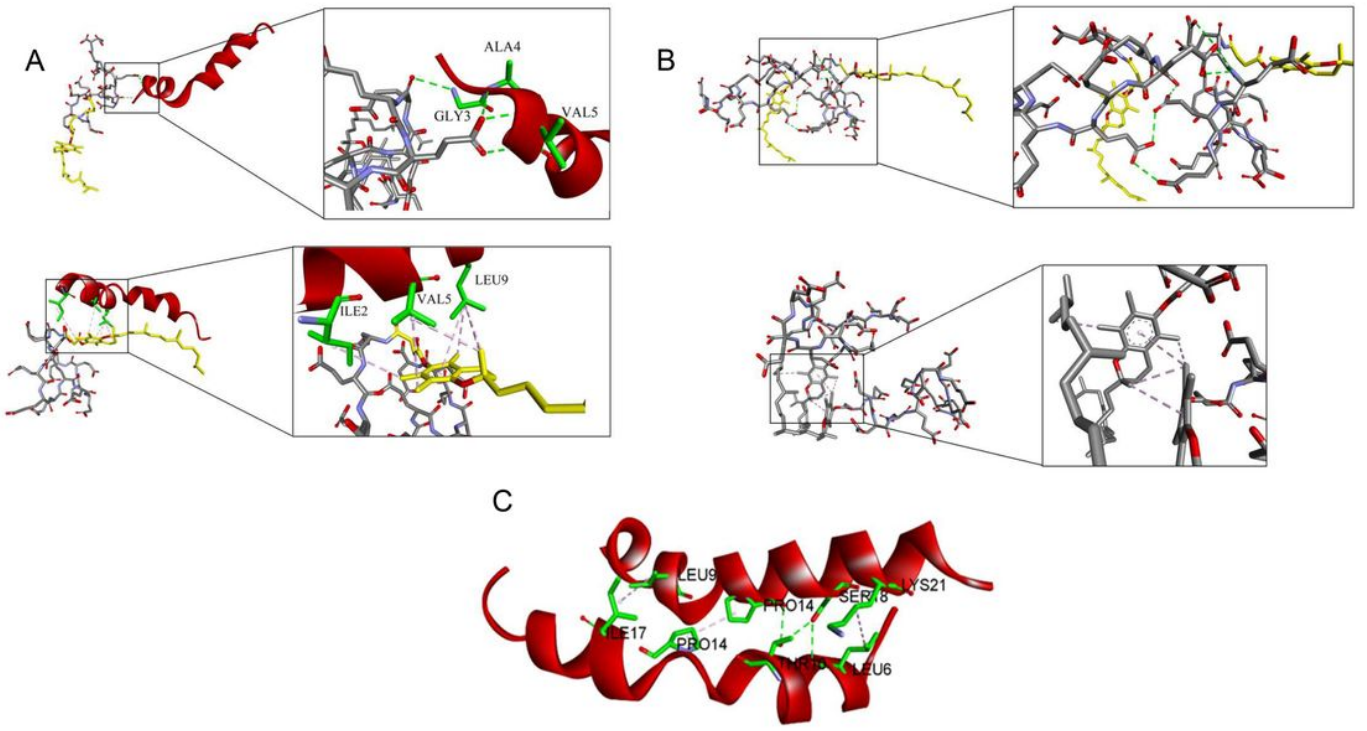

Figure 3

Interactions between melittin and VG (A), VG and VG (B), melittin and melittin (C) mainly based on hydrogen bonds (green) and stacking interaction (pink).

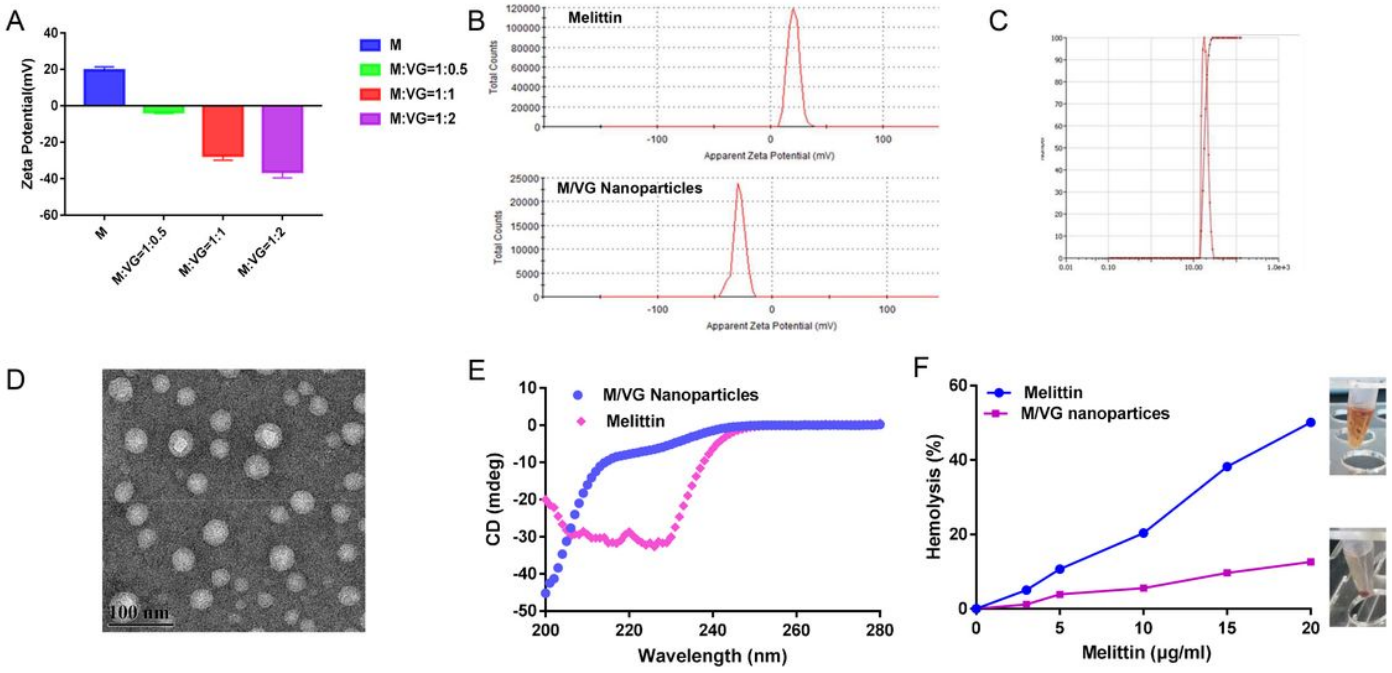

Figure 4

Zeta potentials of different molar ratios of melittin/VG (A). Zeta potentials of melittin and melittin/VG (mole ratio 1:1) (B). Hydrodynamic size (C) and transmission electron micrograph (D) of M/VG nanoparticles. Circular dichroism (E) spectral observation of M/VG nanoparticles. Hemocompatibility of M/VG nanoparticles (F).

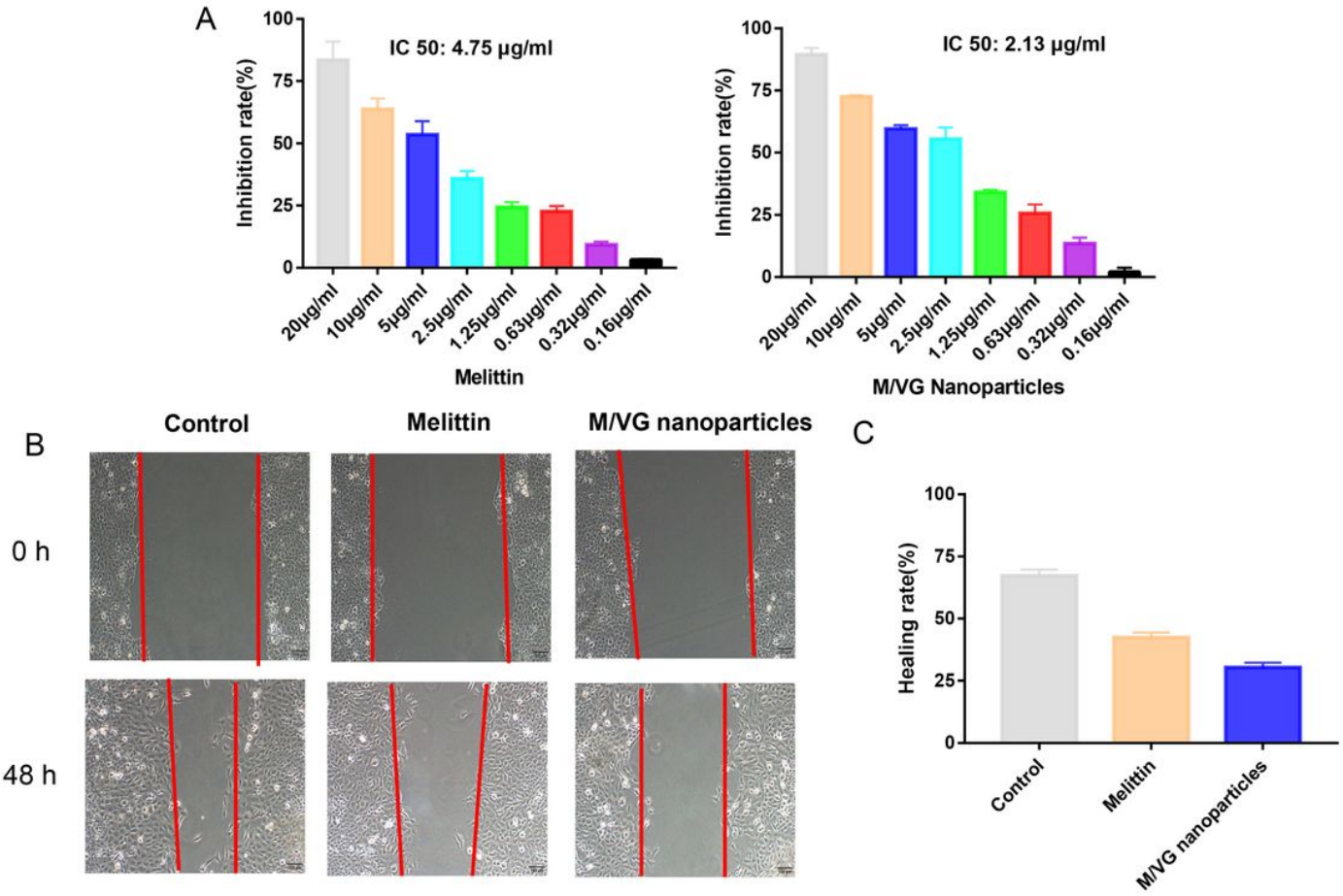

Figure 5

Viability (A) and motility (B) of HepG2 cells after treatment with melittin or M/VG nanoparticles for 48 h. Quantitative analysis of healing rate for melittin or M/VG nanoparticles (C).

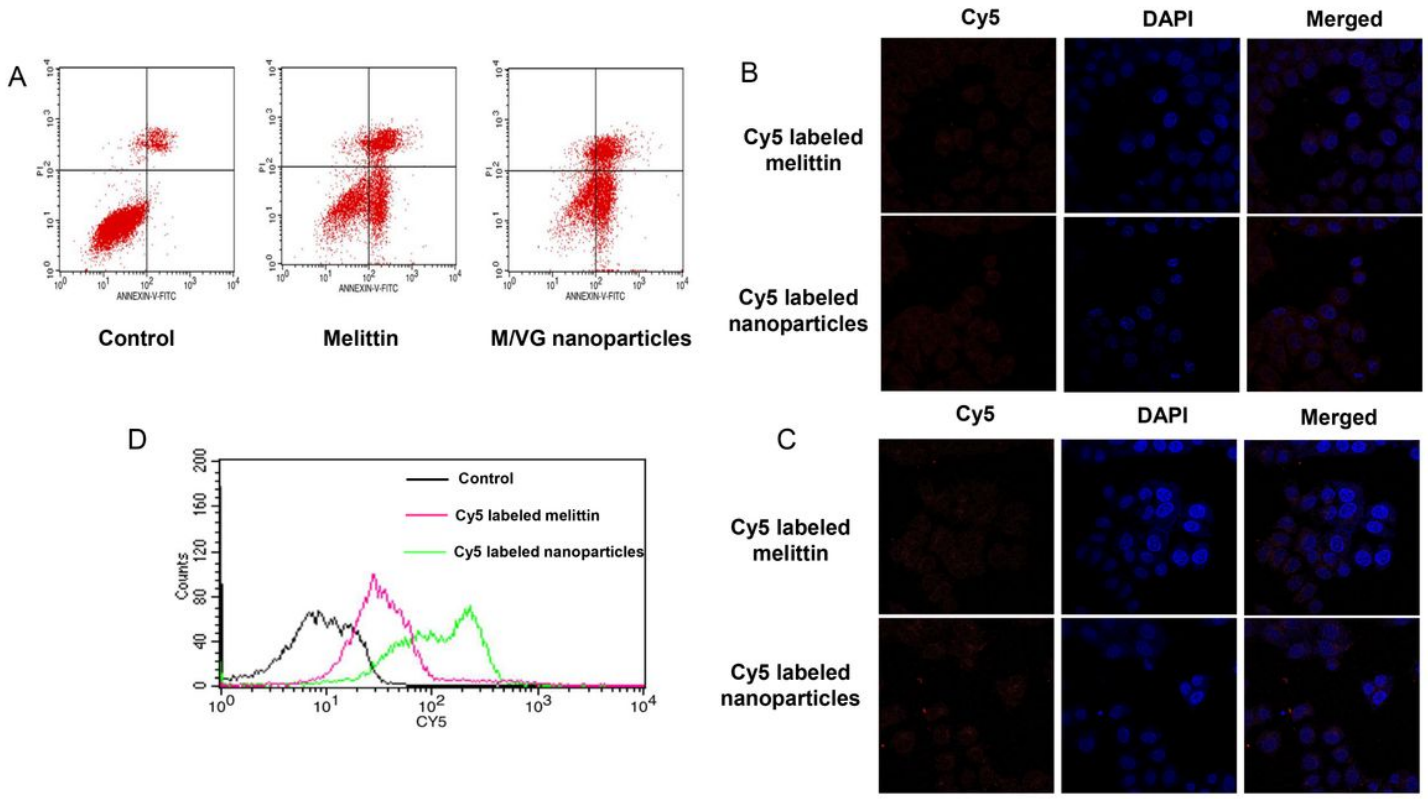

Figure 6

Apoptosis analysis (A) of HepG2 cells after treatment with melittin or M/VG nanoparticles for 48 h. Cellular uptake at 1 h (B) or 4 h (C) and its quantitative analysis at 4 h (D) of Cy5-labeled melittin and Cy5-labeled nanoparticles.

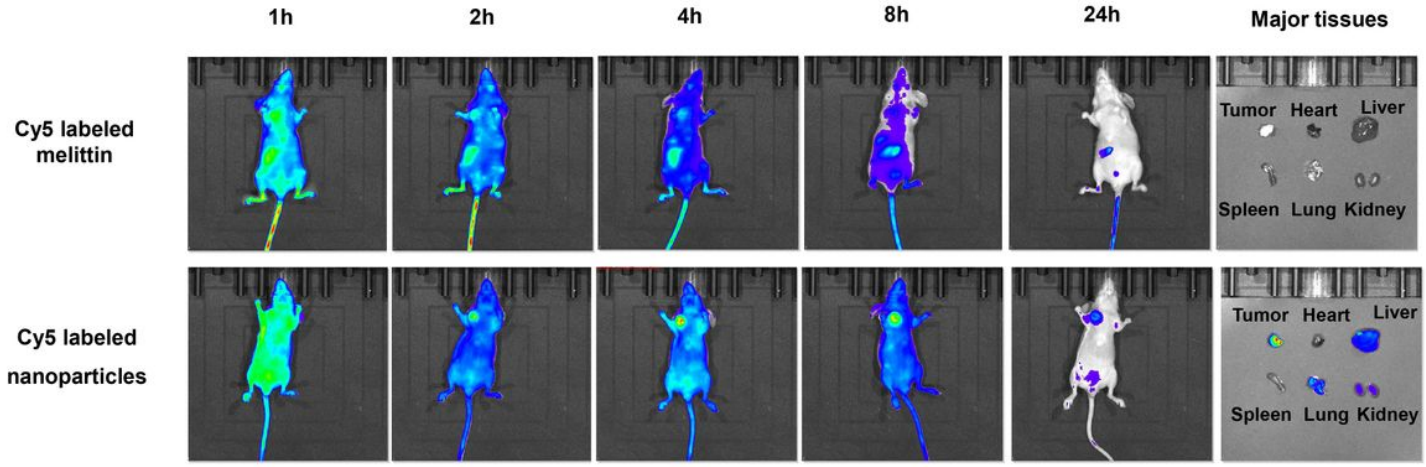

Figure 7

In vivo targeted imaging of Cy5-labeled melittin and Cy5-labeled nanoparticles.

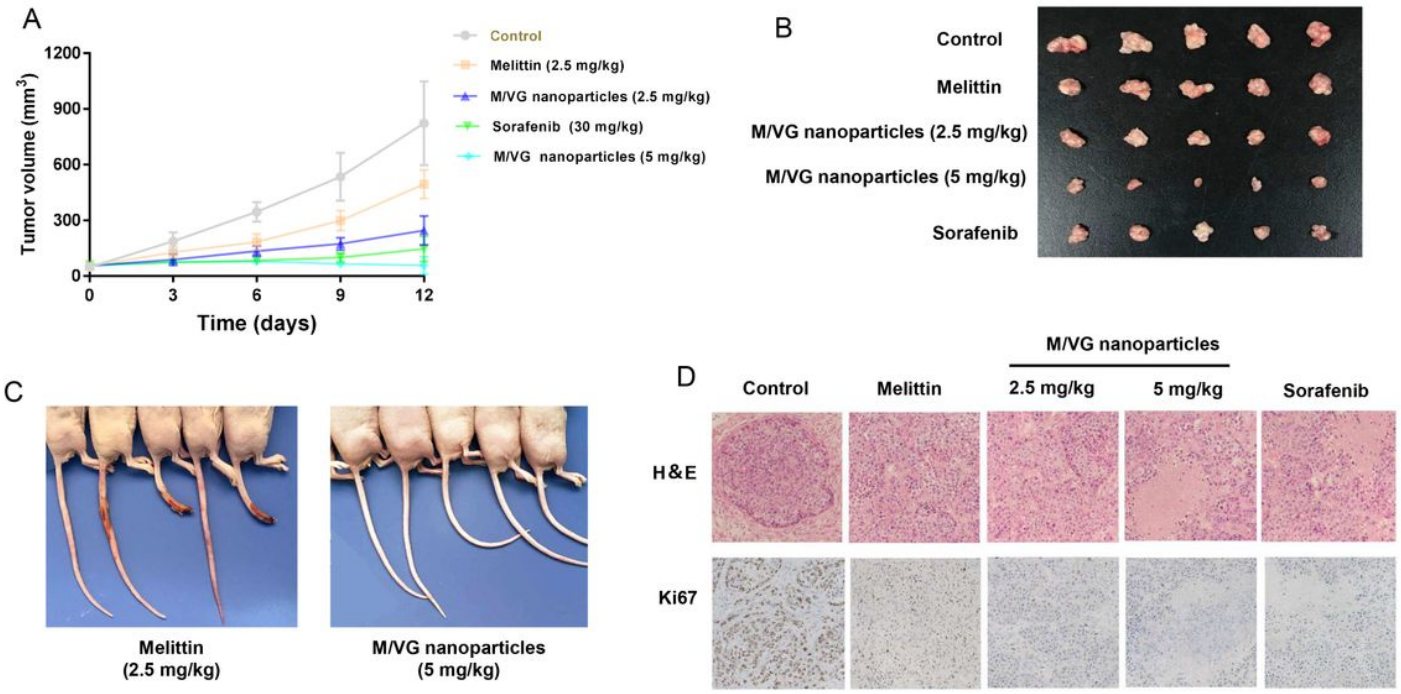

Figure 8

Tumor growth curve (A) and tumor images at the end of the experiment (B) for different treatments. Injury of tails observation of melittin (2.5 mg/kg) and M/VG nanoparticles (2.5 mg/kg) at the end of the experiments (C). H&E and Ki67 staining of tumor tissues (D).

Figure 9

H&E of the heart, liver, spleen, lung, and kidney for *in vivo* anti-tumor evaluation of all groups.

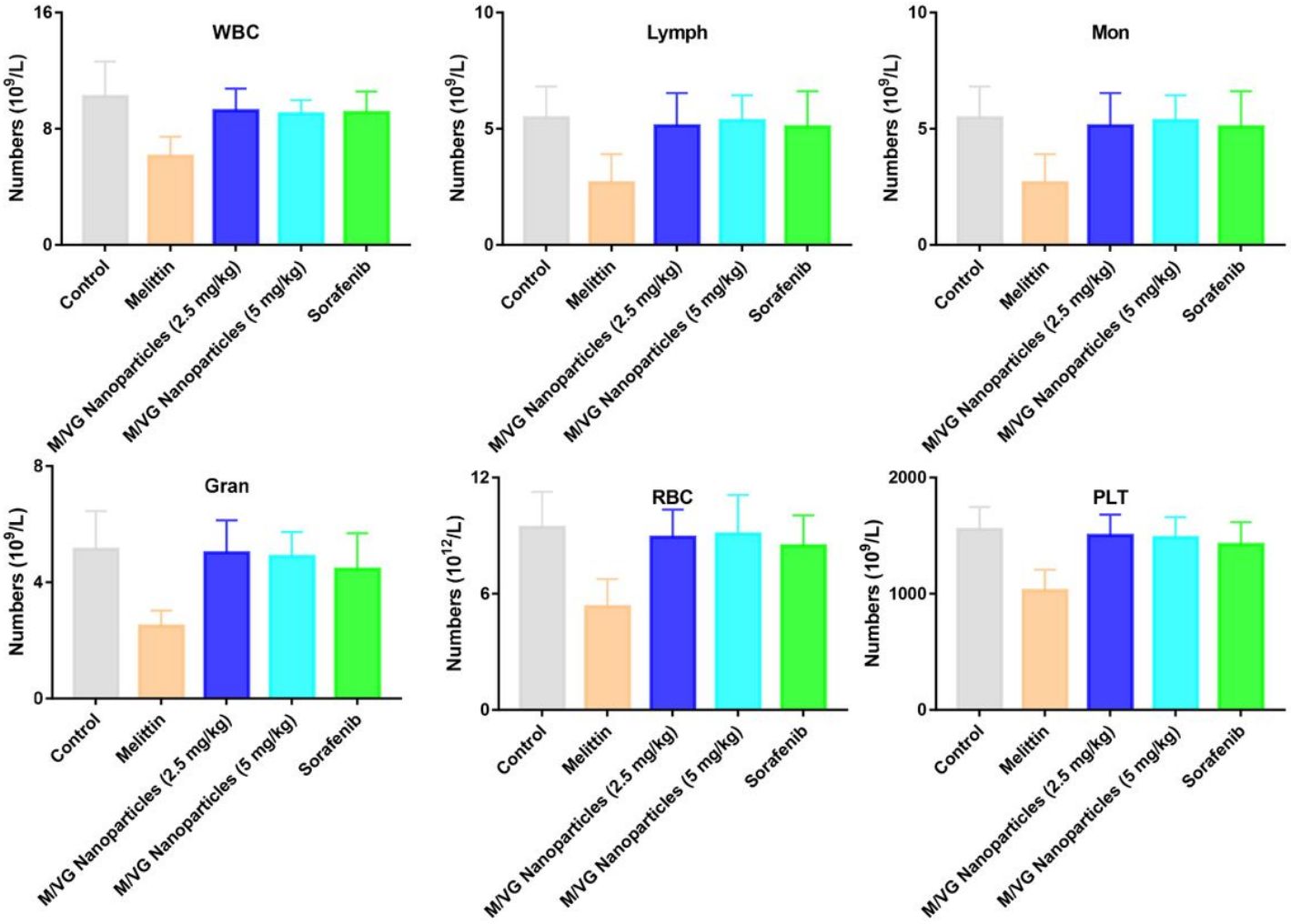

Figure 10

Hemocyte levels of all groups at the end of *in vivo* anti-tumor evaluation.

Supplementary Files

This is a list of supplementary files associated with this preprint. Click to download.

- GraphicAbstract.jpg